AIAA JOURNAL
Vol. 50, No. 10, October 2012

Dynamic Stall Control Using Deployable Leading-Edge Vortex Generators

A. Le Pape,* M. Costes,* F. Richez,* G. Joubert,† F. David,‡ and J.-M. Deluc§
ONERA–The French Aerospace Lab, F-92190 Meudon, France

DOI: 10.2514/1.J051452

A new concept of active dynamic stall control is proposed, designed and experimentally tested on a OA209 airfoil model. The active control principle is based on leading-edge vortex generation in order to alleviate the dynamic stall vortex formed and convected at the leading-edge of an airfoil operating at a helicopter blade in fast forward flight. The active device aims to be used only during retreating blade side for dynamic stall flight conditions in order to avoid drag penalties on the advancing blade side. The designed actuator is a row of deployable vortex generators (DVGs) located at the leading-edge of the airfoil that fit the airfoil shape when retracted. Deployment is possible for different heights as well as different phases and frequencies with respect to the airfoil oscillation. The paper addresses the validation of the effectiveness of the devices to delay static stall and alleviate dynamic stall penalties. Results show a delay in static stall angle of attack of 3 deg and a reduction of negative pitching moment peak up to 60% for dynamic stall. The analysis of the experimental database indicates that different compromises between lift and pitching-moment can be achieved depending on the phase actuation of the DVGs.

Nomenclature

Cd	=	drag coefficient
Cl	=	lift coefficient
Cm	=	pitching-moment coefficient
c	=	airfoil chord length, m
e	=	deployable vortex generator spanwise spacing, mm
f	=	airfoil pitching oscillation frequency, Hz
$hDVG$	=	deployable vortex generator deployment height, mm
k	=	airfoil pitching oscillation reduced frequency based on half-chord
M	=	Mach number
Re	=	Reynolds number based on the airfoil chord c
α	=	angle of attack, deg

I. Introduction

HELICOPTER rotor blades encounter a wide range of aerodynamic conditions during cruise flight, varying from transonic flow, with moderate angles of attack on the advancing blade side, to low subsonic flow, with large angles of attack on the retreating blade side. With increasing cruise speed, angles of attack above static stall are reached on the retreating blade side. The cyclic pitching motion of the blade then leads to dynamic stall that induces large unsteady loads. In particular, large negative (nosedown) pitching moments are observed during dynamic stall and induce large impulsive pitch-link loads that can damage the control command of the helicopter. Dynamic stall may appear in several flight conditions, such as high-speed forward flight or maneuvers, and it strongly limits the flight envelope of the rotorcraft. Therefore, dynamic stall-related topics have been an intensive area of research in the last decades to improve the understanding of the complex physical phenomena involved, and dynamic stall remains a very tough problem in aerodynamics. The alleviation of dynamic stall on rotorcraft blades has also been an area of investigation for numerous researchers. Since structural problems associated with dynamic stall are due to negative pitching moments induced by the shedding of the strong leading-edge dynamic stall vortex, the objective of the dynamic stall control is primarily to reduce the negative pitching moment while maintaining a similar mean and maximum achievable lift. The reduction of drag due to dynamic stall is generally considered as a secondary objective; any reduction of dynamic stall will lead to an extension of the flight envelope.

Several devices have been proposed, and for some of them, experimental validation has been demonstrated on two-dimensional (2-D) wind-tunnel models. Dynamic stall is linked with the shedding of a strong leading-edge dynamic stall vortex, and therefore, most authors proposed devices acting at the airfoil leading edge. Suction at the leading-edge [1], blowing [2,3], and plasma actuation using dielectric barrier discharge (DBD) actuators [4] were, for example, demonstrated to bring some benefits. Large modifications of the airfoil shape were also investigated using a deforming leading edge [5], a droop leading-edge airfoil [6,7], or leading-edge slats [8]. However, all of these devices face the problem of possible future integration into a rotor blade, the rotating environment, and centrifugal forces, which impose huge design constraints on the blade and on the suggested active dynamic stall control devices. The most promising studies concern the delay of dynamic stall or its alleviation using vortex generators. Significant dynamic stall reductions with leading-edge vortex generators were experimentally demonstrated by Martin et al. [9] and Mai et al. [10]. In this last study, the devices are small flat cylinders glued at the airfoil leading edge. However, even if the leading-edge vortex generators are located near the stagnation point so that the flow is not affected at low and moderate angles of attack, the device may cause penalties for nonstalled flight conditions. Active flow control solves this problem, and for example, pulsed-jet vortex generators [11,12] were also successfully used, with one major drawback being the requirement for additional air supply.

The paper presents an innovative active device proposed and experimentally validated by the authors in order to alleviate dynamic stall penalties based on leading-edge vortex generation. The active device aims to be used only on the retreating blade side for dynamic stall flight conditions in order to avoid drag penalties on the advancing blade side; an actuation at a typical helicopter rotational frequency (one per revolution) is thus foreseen. The actuator is a row of deployable vortex generators (DVGs) located at the very leading edge of the airfoil (Fig. 1). The vortex generators are small blades that fit the airfoil leading-edge shape so that, when retracted, the airfoil is

Received 24 June 2011; revision received 27 January 2012; accepted for publication 17 March 2012.

*Research Scientist, Applied Aerodynamics Department.
†Ph.D. Student, Applied Aerodynamics Department.
‡Test Engineer, Aeroelasticity and Structural Dynamics Department.
§Test Engineer, Fauga-Mauzac Wind Tunnels Department.

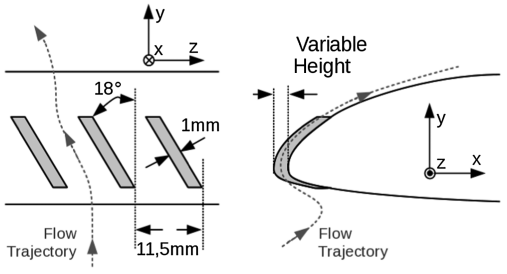

Fig. 1 Sketch of designed deployable vortex generator system.

clean. The DVGs can be deployed at various heights (from 0.1 to 3 mm with an accuracy of 0.05 mm) and with various deployment motions (sine, square) with respect to the airfoil pitching motion. Previous works have been performed on flow control using deployable vortex generators such as boundary-layer separation control, presented in [13], or the effect of vortices generated by dynamic vane vortex generators (VGs) on the turbulent boundary layer in [14]. Seshagiri et al. also investigated in [15] static and active vortex generators to improve the airfoil maximum lift coefficient at low Reynolds numbers. In complement to these studies, the current work presents a new application of deployable vortex generators to an airfoil in pitching oscillation motion under dynamic stall conditions. The objective here is not to dynamically generate vortices on a static airfoil configuration but to deploy, when needed, the VGs on an oscillatory airfoil.

The DVGs have been designed and implemented in an OA209 airfoil model and tested in the ONERA F2 low-speed wind tunnel for static stall and dynamic stall conditions. The DVG system design, as well as the experimental setup, is first introduced. Several DVG heights and control schemes have been tested to alleviate dynamic stall penalties. These experimental investigations of DVG devices for dynamic stall control are fully described in the paper. Static stall and dynamic stall results with various DVG deployment schemes are then presented and discussed.

II. Description of the Operating Principle and Design of the Deployable Vortex Generators

Previous numerical and experimental studies on the OA209 airfoil under static and dynamic stall conditions suggest the following conclusions:

1) At low and moderate Mach numbers and Reynolds numbers between 1 and 2 million, the OA209 airfoil experiences a leading-edge static stall [16].

2) A laminar separation bubble develops on the suction side of the airfoil for high angles of attack before stall [16,17].

3) The laminar separation bubble and the laminar-turbulent transition play a role in the static and dynamic stall for these aerodynamic conditions [18,19].

4) A large leading-edge vortex is emitted at dynamic stall and induces a strong pitching-moment stall [16,18,19].

An extensive literature review of previous dynamic stall control studies led to the choice of a simple, versatile mechanical system located at the leading edge of the airfoil. The idea is to use classical vortex generators in order to delay stall but to make these vortex generators deployable: when the flow is attached, the vortex generators are hidden inside the model so that the model is clean (no drag penalty); when higher angles of attack are reached and the model is about to stall, the vortex generators can be activated to delay stall.

The principle of the proposed active device for dynamic stall control is to use these deployable vortex generators in order to trigger the laminar-turbulent transition and then, once the boundary layer is turbulent, to control it in order to delay the stall. This could be achieved by a progressive increase of the height of the vortex generators' deployment with respect to the airfoil pitching oscillations. In the current experiment, the aerodynamic conditions are close to the one experienced by a full-scale helicopter blade in forward flight, and the establishment time of the vortex emitted by the device is expected to be an order of magnitude lower than the period of oscillation. Indeed, for an airfoil chord of 0.5 m and an upstream velocity of 55 m/s, the convection time of a vortex emitted at the leading edge over the airfoil chord is $t_{\text{conv}} = \sim 0.01$ s. The period of the oscillation for a half-chord-based reduced frequency equal to 0.1 is $t_{\text{osc}} = \sim 0.3$ s. Therefore, the DVGs are expected to affect the flowfield very quickly once deployed, and the phase-lag effect with respect to airfoil oscillation is probably negligible. This observation is confirmed by the fact that the dynamic stall vortex is generated at the leading edge.

Based on boundary-layer computations at the leading edge for attached flow for the prestall angle of attack (AOA), the boundary-layer thickness is approximately $\delta = 0.3$ mm at $x/c = 1\%$ upstream of the laminar separation bubble and $\delta = 1$ mm downstream of the bubble at a 15 deg angle of attack for a Reynolds number equal to 1.8 million and incoming Mach number of 0.16. Usually, vortex generators are designed to generate a vortex at the limit of the boundary layer to promote its mixing with the external flow. Vortex generator height is generally chosen equal to the displacement thickness of the boundary layer or even below this value [20]. In our case, the boundary-layer thickness varies with the airfoil angle of attack. However, dynamic stall is known to lead to a strong and brutal separation linked with the shedding of an intense vortical structure at the leading edge: the dynamic stall vortex. Thus, a higher DVG height is expected to be required to generate a stronger vortex in the separating shear layer. The DVG system (Fig. 1) was thus designed so that heights from 0.1 to 2.7 mm can be achieved with an accuracy of 0.05 mm. Small DVG heights can be set to follow the boundary-layer thickness, but large DVG heights outside the boundary-layer thickness can also be achieved to generate strong vortices in the separating shear layer. The DVGs' shape has been designed in order to fit the OA209 leading-edge airfoil shape when retracted. The device chord length is $e = 10$ mm. The DVGs' thickness is imposed by stiffness constraints in order to activate the DVGs, leading to a thickness of 1 mm. A row of corotative DVGs, spaced at 11.5 mm and oriented with an angle of 18 deg with respect to the freestream, is chosen. Device spacing and angle have been chosen based on a literature review and, in particular, in comparison to the parameters gathered by Lin in his review [20]. With an expected range of heights ($hDVG$) between 0.3 and 2.7 mm and a spacing $e = 11.5$ m, the height to spacing ratio $e/hDVG$ varies between 38 and 4, which is in the range of the usual height to spacing ratio for such devices. In [10], Mai et al. show, for example, good aerodynamic performance of their leading-edge vortex generators on the same airfoil with height to spacing ratios of 18 and 38. Similar parameters ($L/h = 57$, $\beta = 18$ deg) were also found to be the most effective for corotating vortex generators in a detailed parametric study performed by Godard and Stanislas in [21].

III. Experimental Setup

A. ONERA F2 Wind Tunnel

The wind-tunnel tests were conducted in the ONERA F2 wind tunnel. This research facility has a test section 1.4 m wide, 1.8 m high, and 5 m long; wind speeds up to 100 m/s can be reached. The wind-tunnel walls are made of glass panels, allowing full optical access and making the F2 wind tunnel particularly suitable for tests that require a detailed flowfield investigation. An onsite laser Doppler velocimetry (LDV) system is available for such measurements. The floor and the ceiling of the test section are equipped with pressure taps for wind-tunnel wall corrections.

The test conditions investigated for this dynamic stall control research are similar to those presented in [16], with the same airfoil and a freestream velocity of 55 m/s corresponding to a Reynolds number based on an airfoil chord equal to 1.8 million.

Fig. 2 OA209 model in F2 wind-tunnel test section.

B. Airfoil Model and DVG System

The deployable vortex generator device has been designed and manufactured at ONERA and has been implemented in an OA209 airfoil model (Figs. 2 and 3). The model has a chord length of 500 mm and a span of 1.4 m, thus giving an aspect ratio of 2.8. In spite of this quite low aspect ratio, surface flow visualization demonstrates a pure 2-D flow around the middle section of the model, extending approximately one-third of the model span at high angles of attack and more than that at low and moderate angles of attack. The full-span model is equipped with 120 DVG blades. The DVGs are actuated by two embedded linear hydraulic motors located at the left- and right-hand sides of the model. A close monitoring of the DVGs' height is ensured by three position sensors located at the linear hydraulic motor positions and at the middle of the model. A Teflon treatment on each DVG blade is applied to limit frictions during the deployment and allow a very small clearance between each DVG blade and the model to be reached. Laboratory tests were performed and demonstrated that the DVGs can be actuated at operational frequencies from one-per-revolution (∼3.5 Hz) to 10-per-revolution (∼35 Hz) for the full range of height deployment. Structural design of the model ensures no interference with the model's natural frequencies which have been evaluated by finite element simulations. The first wing model mode is computed around 90 Hz for a flexion mode, and the chordwise in-plane mode of the DVG system is evaluated to be equal to 140 Hz.

The OA209 model is instrumented with 77 unsteady pressure sensors. Thirty-seven Kulites are located at midspan and 2×20 Kulites are located at ± 200 mm from the midspan on the airfoil suction side in order to identify possible three-dimensional (3-D) flows. Aerodynamic coefficients are obtained from Kulites integration along the model centerline. Unsteady pressures are acquired at 2048 Hz over 30 s, which corresponds, for the nominal model oscillation frequency (one-per-revolution = 3.5 Hz), to 105 oscillation cycles with a time discretization of 585 points per cycle. The model pitching motion is driven by rotating hydraulic motors, located on the right- and left-hand sides of the wind-tunnel test section, that allow a static angular displacement from −5 to 22 deg with a maximum dynamic amplitude of 7 deg at the nominal frequency of 3.5 Hz. The airfoil motion and angle of attack are determined by two angular displacement sensors in each hydraulic motor and three accelerometers inside the model. The accuracy of the angle of attack is estimated at 0.025 deg.

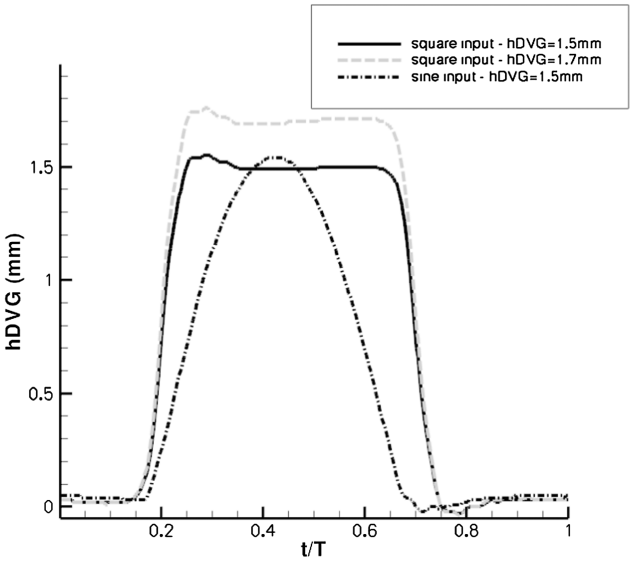

Fig. 4 Examples of DVG deployment for square and half-sine input signals.

Examples of DVG deployment are plotted in Fig. 4 for different DVG motion input signals. Very good accuracy is observed for the maximum height for both square and half-sine inputs. For square inputs, a small overshoot (less than 0.05 mm) is observed when DVGs are deployed. Considering the very short establishment time, this overshoot is negligible. The measurement of DVG height for half-sine input is very smooth, and no staircasing is observed in the DVG deployment. The DVG control system is very satisfactory, with very good accuracy of the maximum height as well as a perfectly controlled deployment.

IV. Static Stall Delay

A first assessment of DVGs' effectiveness was performed for the OA209 airfoil under static stall. Various DVG heights were tested from 0.3 to 2.5 mm. Lift and pitching-moment polar curves are presented in Fig. 5. The clean case ($hDVG = 0$ mm) is plotted in black and presents a sharp leading-edge stall at an angle of attack of 15 deg. For an $hDVG$ equal to 0.3 mm, a delay of this leading-edge stall by 1 deg is observed, keeping the maximum lift at the same level as the clean case. This height corresponds approximately to the boundary-layer thickness at the DVG blade trailing edge. Pressure distributions at a 15-deg angle of attack (Fig. 6) show a much higher suction peak for $hDVG = 0.3$ mm than in the clean case. At a slightly higher height ($hDVG = 0.5$ mm), the static stall angle of attack is the same as that of the clean airfoil but with a slight degradation of the maximum lift. Stall delay is then observed for heights from 1 to 1.7 mm. A maximum delay of 3 deg of lift and pitching-moment stall is observed for $hDVG = 1.5$–1.7 mm. The lift polar curve presents a typical shape of trailing-edge stall for these

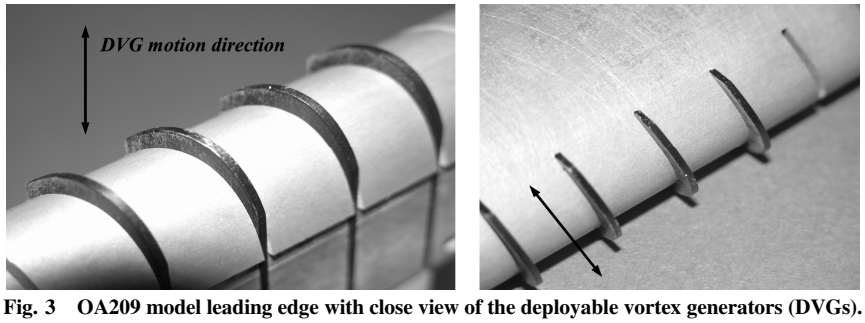

Fig. 3 OA209 model leading edge with close view of the deployable vortex generators (DVGs).

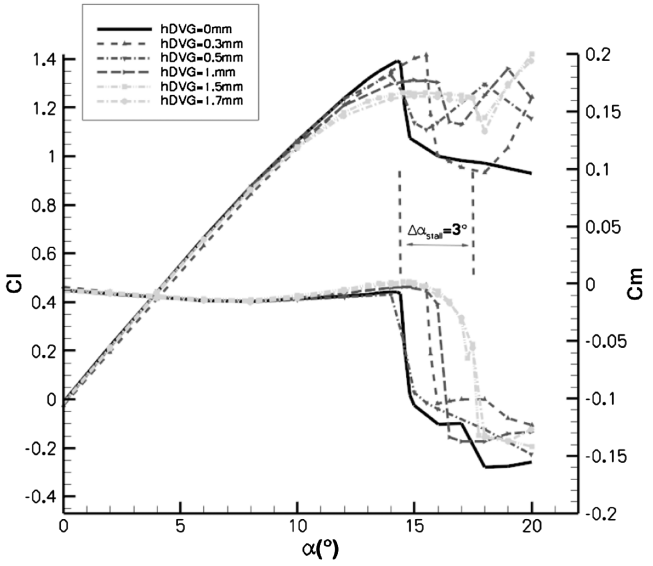

Fig. 5 Static stall delay obtained for various DVG heights.

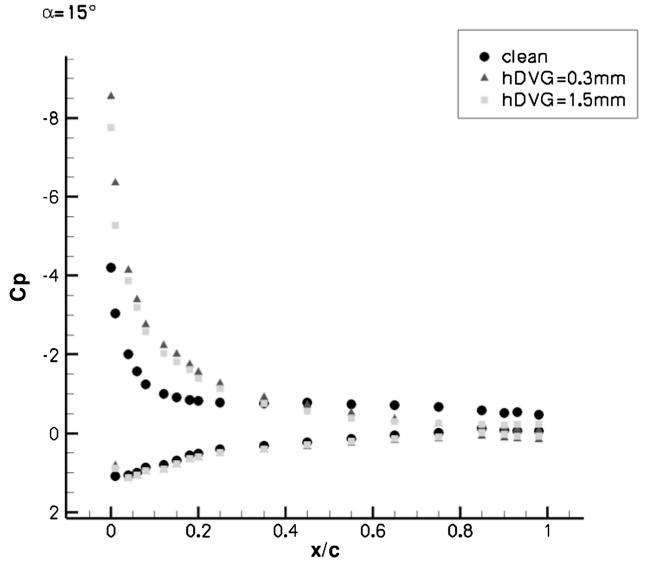

Fig. 6 Pressure distribution for different DVG heights at $\alpha = 15$ deg.

heights, with a reduction of the slope at the prestall angle of attack, and then a smooth stall appearance. This promotion of a trailing-edge stall implies the loss in maximum lift observed in Fig. 5.

While increasing $hDVG$, the static stall progressively shifts from a sharp leading-edge stall to a shallow trailing-edge stall. The LDV measurements performed for an angle of attack of 16.7 deg in the leading-edge region (Fig. 7) show that the leading edge remains attached with the DVGs activated when the flow separates in the clean case.

Oil flow visualizations for a prestall angle of attack (14 deg; Fig. 8) show that the trailing-edge separation is more pronounced with the DVGs. This qualitative visualization also shows good 2-D flow conditions for $hDVG = 0$ mm and allows following the traces of the vortices for $hDVG = 1.5$ mm.

An increase in drag is obviously expected when the DVGs are deployed for prestall angles of attack. Indeed, wake measurements were performed for two DVG heights for various angles of attack up to 15 deg. Results are compared with the measurements for $hDVG = 0$ mm and with reference experimental results obtained previously with a clean OA209 model (Fig. 9). A first observation is that, when the DVGs are not deployed, no additional drag is produced for $hDVG = 0$ mm in comparison to a fully clean model. At low angles of attack, an increase of drag is observed for $hDVG = 1$ and 1.5 mm. Both heights lead to a similar increase of 15% of the total drag. At higher angles of attack, the drag is increased by 20% for DVGs deployed at 1 and 1.5 mm. Additional drag is, indeed, produced by the device itself, but it is also produced by the larger trailing-edge separation. No measurements are available for higher angles of attack, in particular, for poststall angles of attack because the wake is too wide to ensure good drag estimation with the wake rake measurement technique. However, as the separation is clearly reduced with DVGs, one can expect drag reduction after stall.

V. Influence of DVG System on Dynamic Stall (Clean Airfoil)

The addition of a mechanical system at the leading edge of an airfoil model may involve aerodynamic perturbations and, therefore, modify the flow. In the case of the DVG system, particular attention has been paid to the manufacturing tolerances in order to have, on the one hand, a perfect match of the DVG with the airfoil when retracted, and, on the other hand, a clearance between the DVG and the airfoil that is as small as possible. For this last point, the objective is to allow the DVG to be deployed while limiting any possible flow leakage between the pressure side and the suction side of the airfoil. Unfortunately, in spite of these efforts, some differences are observed between an absolutely clean leading edge and the leading edge with the DVG system with $hDVG = 0$ mm. Lift and pitching-moment

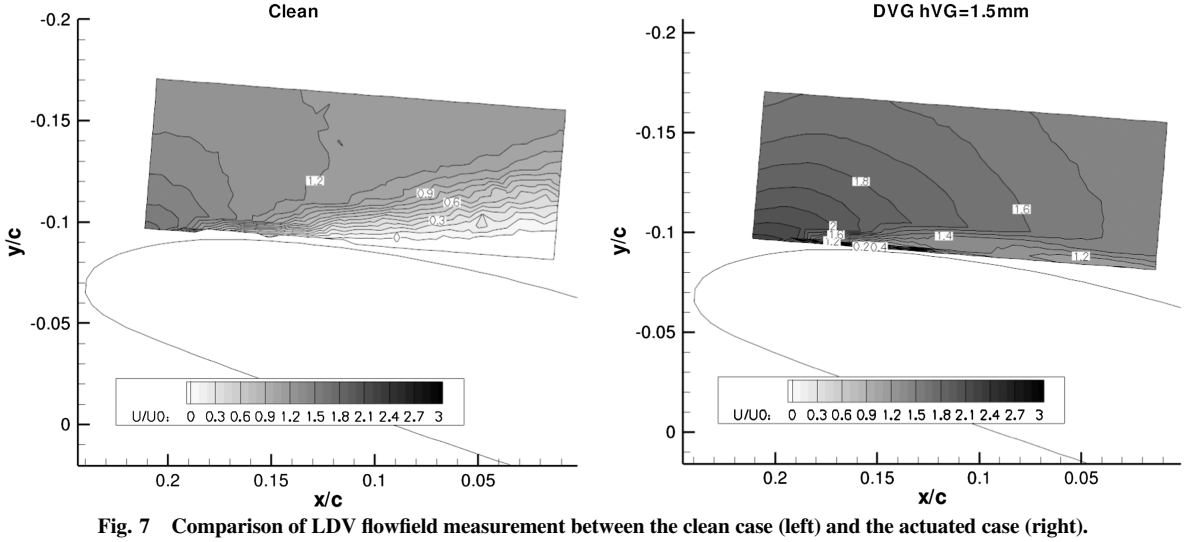

Fig. 7 Comparison of LDV flowfield measurement between the clean case (left) and the actuated case (right).

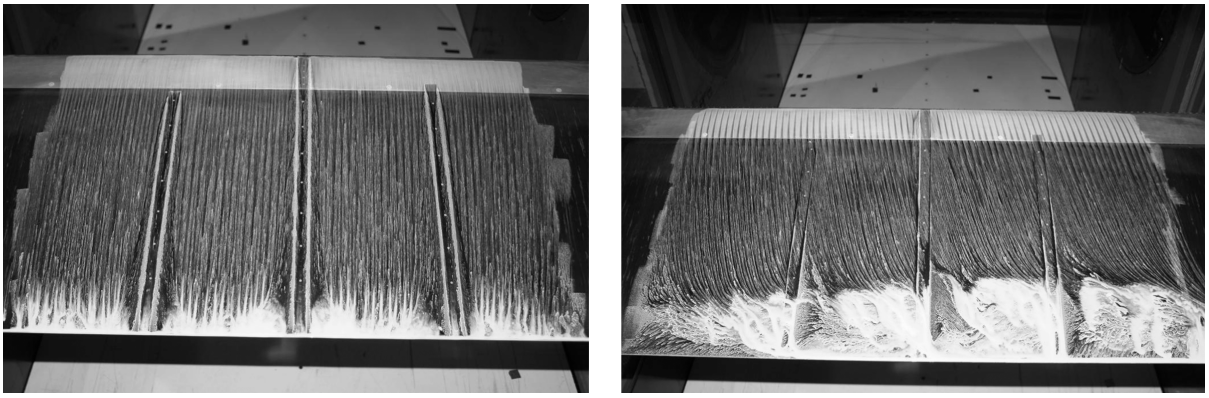

Fig. 8 Oil flow visualization, $\alpha = 14$ deg: $hDVG = 0$ mm (left); $hDVG = 1.5$ mm (right).

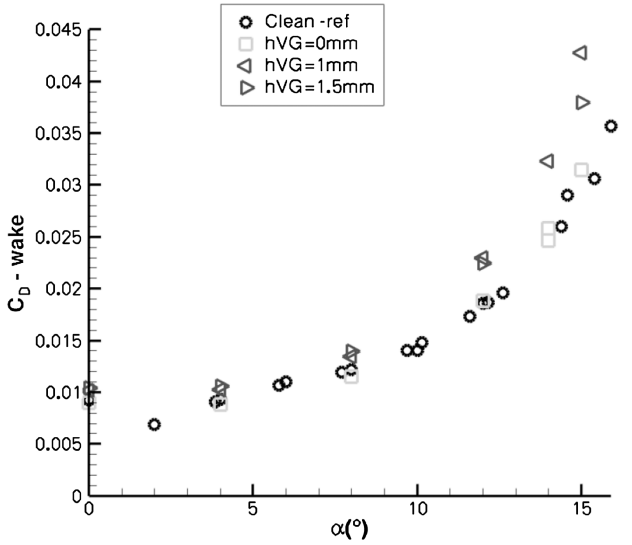

Fig. 9 Total drag coefficient measurements for static stall.

hysteresis comparisons are presented in Fig. 10. Differences can clearly be seen around the maximum angle of attack region when the airfoil stalls, as well as during the reattachment process. A closer examination of the pressure distributions during the oscillation cycle shows that the stall appears slightly earlier in the $hDVG = 0$ mm case. Furthermore, the $hDVG = 0$ mm case reattaches earlier and does not present the slope inflexion that can be observed during the downstroke for the clean case. The small roughness at the leading edge and the possible leakage due to the DVG system have, therefore, some influence on the flow. A hypothesis to explain the origin of these differences is the perturbation of the natural laminar-turbulent transition in the $hDVG = 0$ mm case. This dynamic stall case is, indeed, known to be very sensitive to transition, with the development of a laminar separation bubble at high angles of attack during the upstroke that is thought to have a role in the stall process [16–18]. The reattachment process has also been demonstrated to be driven by laminar-turbulent transition using numerical simulations [19].

However, the maximum lift and minimum negative pitching-moment values are very close for both cases. These values are used in the following paragraphs as metrics for assessing the dynamic stall alleviation (negative pitching-moment peak) and preservation of nominal dynamic stall characteristics (maximum lift). In spite of flow property differences, these min/max values are almost identical, and the $hDVG = 0$ mm case is used as a reference in the following paragraphs.

VI. Dynamic Stall Alleviation

The DVGs' effectiveness is then demonstrated for a dynamic stall case. A sinusoidal oscillation of the airfoil ($\alpha = 13 \pm 5$ deg) is forced at a reduced frequency based on half the airfoil chord, $k = 0.1$ ($f = 3.5$ Hz): dynamic stall generally occurs on the retreating side of helicopter blades at different azimuth positions and spanwise locations, leading to reduced frequencies based on local incoming flow velocity and the blade half-chord between 0.05 and 0.2. A reduced frequency of 0.1 is a common value for generic dynamic stall [22] and has been chosen for the current investigation.

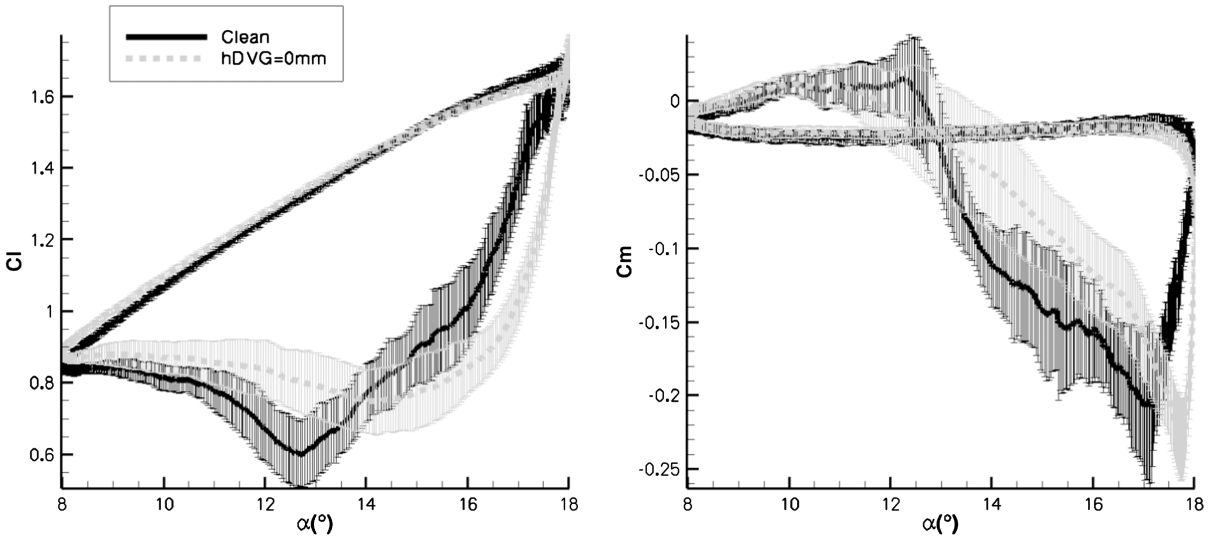

Fig. 10 Lift (left) and pitching-moment (right) hysteresis comparisons between clean and $hDVG = 0$ mm cases.

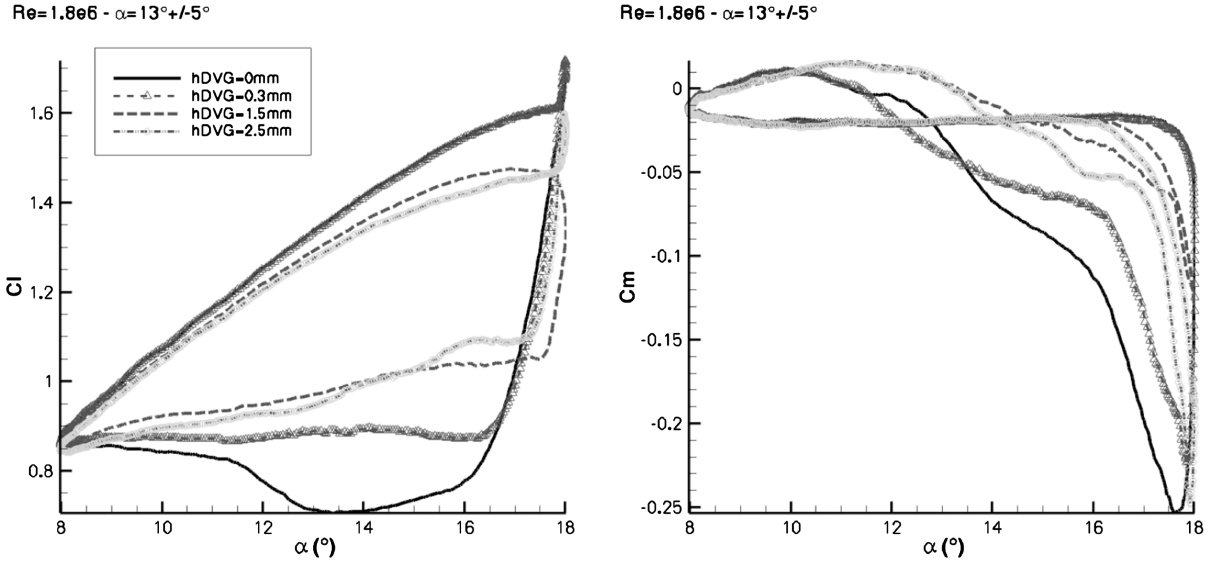

Fig. 11 Lift (left) and pitching-moment (right) hysteresis obtained for various DVG heights.

In the next paragraphs, we define the DVGs actuation duty cycle as the ratio between the time during which the DVGs are activated and an oscillation time period. A duty cycle of 100% corresponds to DVGs that are deployed all over the oscillation cycle. The general objective of this experiment is first to demonstrate that DVGs can reduce the dynamic stall penalties and then to demonstrate that the duty cycle can be minimized (possible actuation power savings, minimization of drag penalties at low angles of attack).

A. Various Prescribed DVG Heights (Duty Cycle Equal to One-Hundred Percent)

Various DVG heights from 0.3 to 2.5 mm are prescribed all over the oscillation cycle; no dynamic deployment of the VGs is considered here. Lift hysteresis and pitching-moment hysteresis loops are plotted in Fig. 11. For increasing $hDVG$, the lift hysteresis loop is reduced. For $hDVG = 0.3$ mm, as for static stall, the lift coefficient is not affected during the upstroke in comparison to the clean case. However, higher lift values are reached during the downstroke in the poststall region, leading to a different reattachment process. For $hDVG = 1.5$ mm, the shape of the hysteresis is totally modified. A deviation in the lift slope is observed during the upstroke at high angles of attack, and the maximum lift coefficient is significantly reduced. The stall is much smoother, and the lift coefficient values during the downstroke are significantly increased in comparison to those of the clean case. Finally, the loss in maximum lift and the improvement during the downstroke are balanced, and the average lift over the oscillation cycle is the same for the clean case and the case with $hDVG = 1.5$ mm. At higher $hDVG$ values, similar hysteresis to the one observed for $hDVG = 1.5$ mm is obtained. The pitching-moment hysteresis evolves in a similar way with respect to increasing DVG height. At low $hDVG$ value, a small reduction of the pitching-moment peak is achieved, whereas a strong reduction of this peak is obtained for $hDVG = 1.5$ mm. Up to this value the negative loop of the pitching-moment hysteresis is progressively reduced with increasing $hDVG$. However, a higher negative pitching-moment peak and a larger negative loop than for $hDVG = 1.5$ mm are observed for $hDVG$ values above 1.5 mm. An optimal value of $hDVG$ can thus be found to minimize the negative pitching-moment peak. Moreover, a compromise has to be chosen between maximum lift reduction and negative pitching-moment peak reduction.

A synthesis of the maximum lift coefficients and the negative pitching-moment peak obtained for varying DVG heights is presented in Fig. 12. Except for very low DVG heights ($hDVG <$ 0.5 mm), a loss of maximum lift is observed (up to 10%). The negative pitching-moment peak is, however, reduced for all DVG heights. Two local minima can be observed. First, at $hDVG =$ 0.3 mm, a small reduction of the negative pitching-moment peak

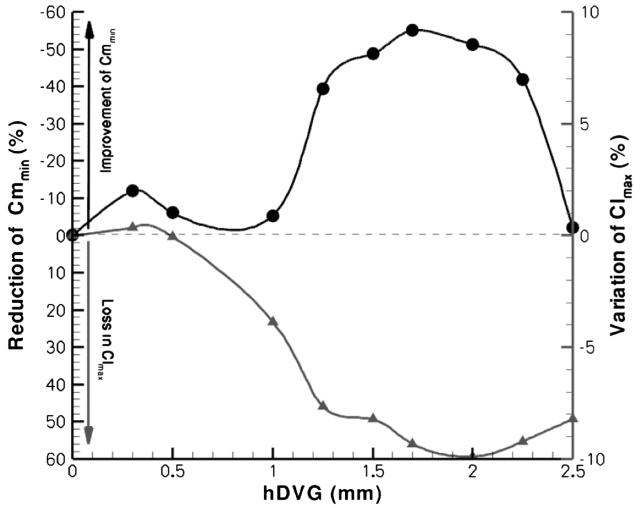

Fig. 12 Synthesis of DVG effectiveness for various heights (duty cycle = 100%).

is obtained, keeping the maximum lift constant. As previously mentioned, this $hDVG$ value is comparable to the boundary layer thickness at the leading edge for prestall angles of attack. However, this reduction of the negative pitching moment is limited ($\sim -15\%$). A second minima with a much larger reduction of the negative pitching-moment peak ($\sim -55\%$) is obtained for DVG heights between 1.5 and 1.7 mm. These values also correspond to the most important loss in maximum lift.

It was decided, for the continuation of the investigation, to focus on the $hDVG$ values that lead to the most efficient alleviation of the dynamic stall penalties. The value of $hDVG = 1.5$ mm was, thus retained for providing a reduction of 50% of the negative pitching-moment peak and limiting the reduction in maximum lift (−7.5%).

For this value, $hDVG = 1.5$ mm, a process similar to that in static stall is at the origin of the dynamic stall reduction. During the upstroke, when the flow is mainly attached in the clean case, the DVGs promote the trailing-edge separation that leads to the deviation of the lift curve slope. At stall and during the downstroke, the DVGs allow the flow to remain attached in the leading-edge region. A leading-edge strong suction peak can, for example, be observed in Fig. 13 for $hDVG = 1.5$ mm, while the flow is totally separated from the leading edge to the trailing edge for $hDVG = 0$ mm.

Figure 13 also shows the comparison of the pressure distribution from the different spanwise stations. For this angle of attack, for which a strong trailing-edge separation is present, one can notice that

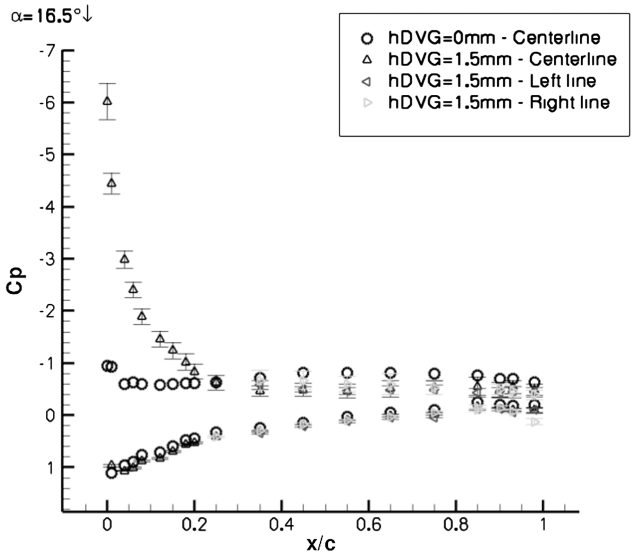

Fig. 13 Pressure distribution comparison for $hDVG = 1.5$ mm at $\alpha = 16.5$ deg (downstroke).

the flow is only slightly 3-D. During the upstroke, there are almost no differences between center, left, and right line measurements (not represented here). However, these conclusions should be cautiously considered: no pressure measurements are available in the leading-edge region in the left and right lines, and the pressure distributions presented are phase-averaged; instantaneous pressure distributions could show higher differences for the different spanwise stations. They are illustrated through error bars in Fig. 13 that correspond to the phase-averaged pressure standard deviation.

The reason for an existing deployment height optimum in DVG effectiveness with respect to negative pitching-moment peak reduction is not yet fully understood. The optimal height, $hDVG=$ 1.5 mm, is unusually above local boundary-layer displacement thickness δ (estimated equal to 0.3 mm at the device location). Recent work by Joubert et al. [23,24] based on numerical simulations suggests that the device thickness has a large influence on the DVG effectiveness. Indeed, the large thickness of the blades (equal to 1 mm), which is required to ensure enough stiffness of the system for the expected deployment frequencies, leads to a DVG shape with a low height-to-thickness aspect ratio. Further investigations are necessary to fully explain the role of the DVG thickness and its probable link with the optimal effectiveness observed for $hDVG = 1.5$ mm.

B. Variable DVG Heights (Duty Cycle Equal to Fifty Percent)

In order to limit the additional drag produced by the DVGs, a control scheme with the DVGs activated only partially during the oscillation cycle is applied. First, the duty cycle is set to 50% (DVGs are deployed during half of the airfoil oscillation cycle), and a parametric study of the phase of the DVGs actuation with respect to the oscillation motion is performed. Zero deg of phase corresponds to DVGs actuated at a mean angle of attack during the upstroke; thus, a phase of 90 deg corresponds to DVGs actuated for the maximum angle of attack of the airfoil. A maximum DVG height of 1.5 mm is chosen for this parametric study, and a square signal input is used for the DVGs actuation.

Results of the actuation phase parametric study are presented in Fig. 14 for lift and pitching-moment evolutions in time over an oscillation cycle in comparison to the reference case ($hDVG$ =0 mm) and the duty cycle = 100% case (solid line, triangle symbol). The results show that, depending on the time the DVGs are actuated, intermediate results from the reference case and duty cycle = 100% case can progressively be achieved. If the DVGs are activated soon enough before the maximum lift and stall (phase = 0 or 40 deg, for example), results are very close to the duty cycle = 100% case. A very strong reduction of the negative pitching-moment peak is observed, but a loss of maximum lift is also obtained. On the contrary, when the DVGs are activated late, after stall and the maximum angle of attack (phase = 120 or 140 deg, for example), the results are very similar to the clean case. This means that the DVGs have a minor influence when they are deployed after stall. In this case, the high maximum lift is preserved, but no reduction of the negative pitching-moment peak is obtained. Only the reattachment process is slightly modified, with marginally higher lift values achieved when the DVGs are deployed (unsteady history effects).

A synthesis of the DVGs actuation phase parametric study is plotted in Fig. 15: the compromise between negative pitching-moment peak reduction (black curve, dot symbol) and variation of maximum lift (gray curve, triangle symbol) is represented for varying actuation phases. The best negative pitching-moment reduction (−50%) is obtained for an anticipated deployment of the DVGs (phase = −40 deg), but in this case, a reduction by 6% of the maximum lift is observed. Maximum lift can be preserved if the DVGs are deployed just before the maximum angle of attack. A small increase of 2% of the maximum lift coefficient is even reached. However, a more limited reduction of the negative pitching moment is then obtained. For a phase actuation equal to 70 deg (just before maximum AOA), a reduction of 30% is obtained for the negative pitching moment, with a small increase of 2% of the maximum lift, which represents a good compromise between these two parameters.

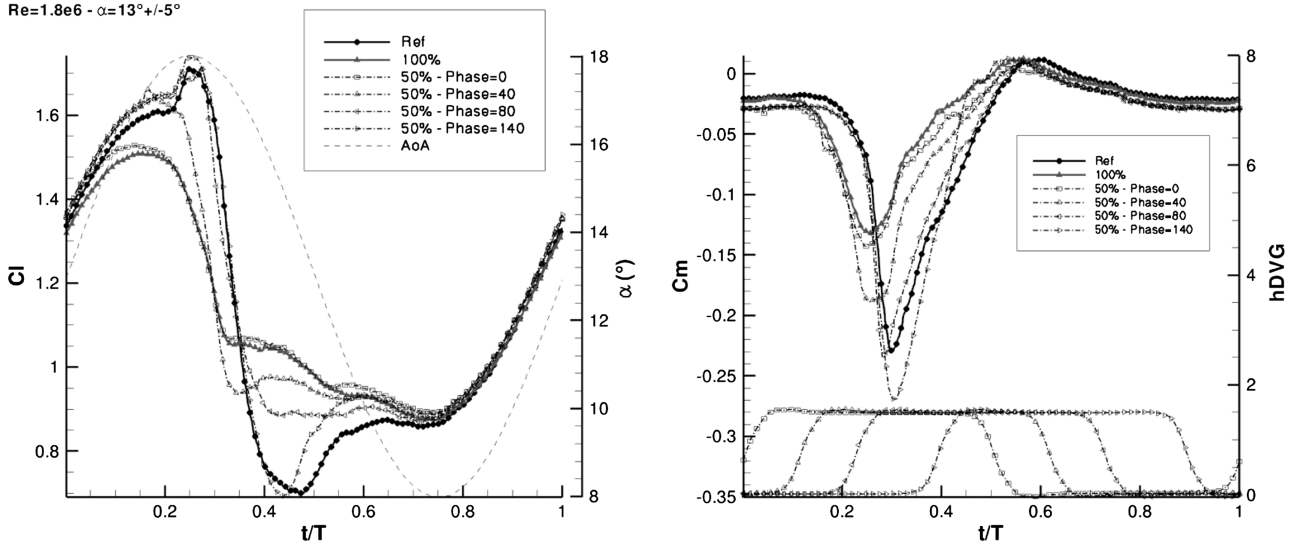

Fig. 14 Lift (left) and pitching-moment (right) hysteresis obtained for $hDVG = 1.5$ mm and various actuation phases.

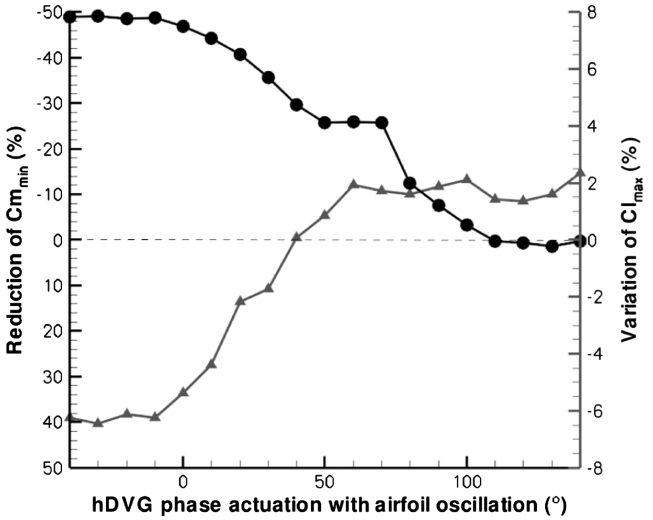

Fig. 15 Synthesis of DVGs effectiveness for $hDVG = 1.5$ mm and various DVGs actuation phases (duty cycle = 50%).

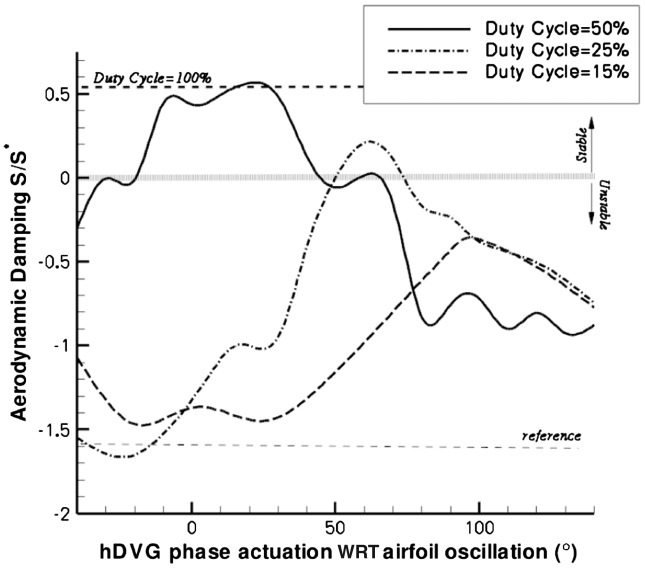

Fig. 17 Aerodynamic damping for $hDVG = 1.5$ mm and several duty cycles WRT DVG actuation phase.

When the DVGs are deployed after the maximum angle of attack, no gain is obtained on the negative pitching moment. A very small increase of the maximum lift coefficient is, however, observed, thanks to the modification of the reattachment process that leads to a higher minimum lift and a small increase of the values of lift during the upstroke. In Fig. 14, it can be, indeed, noticed that the lift curve slope of cases with phase = 100 and 120 deg is higher than in the reference case and that the maximum lift is also slightly higher. This historclights the important unsteady effects in the dynamic stall phenomenon.

C. Duty Cycle Optimization

The previous section shows that significant reductions in dynamic stall penalties can be achieved with DVGs actuated during half of the airfoil oscillation cycle for $hDVG = 1.5$ mm and that different compromises between lift and pitching-moment characteristics can be obtained depending on the phase actuation. The objective of this section is to evaluate if the duty cycle of the actuation can be lowered to limit the additional drag produced by the DVGs. For this, the same parametric investigation as above was repeated with smaller duty cycles (25 and 15%) for the same $hDVG = 1.5$ mm and square inputs for the DVGs actuation.

Results are presented in Fig. 16 for negative pitching-moment peak reduction and maximum lift coefficient variation. Plots for a duty cycle of 25 and 15% are added to the results with a duty cycle equal to 50%. For a duty cycle of 25%, very similar reductions of the negative pitching-moment peak can be obtained as for a duty cycle of 50%. The static deployment case (duty cycle = 100%) is also represented by a dashed line in Figs. 16 and 17.

If the DVGs are deployed early enough and if the duration of the deployment goes beyond the maximum angle of attack (phase = 20 deg, for example), a reduction of 50% of the negative pitching-moment peak is reached with a loss of maximum lift around 6%. However, for the 25% duty cycle, the range for which a good compromise can be found between maximum lift and minimum pitching moment is narrower than for a duty cycle equal to 50%. For a shorter duty cycle of 15%, the range for which benefits can be obtained is even narrower, and only a maximum of 38% of negative pitching-moment peak reduction can be achieved. Indeed, the DVGs have to be deployed before the maximum angle of attack and the stall appearance, but the duration of the DVGs actuation must also last at least until this maximum angle of attack to act efficiently.

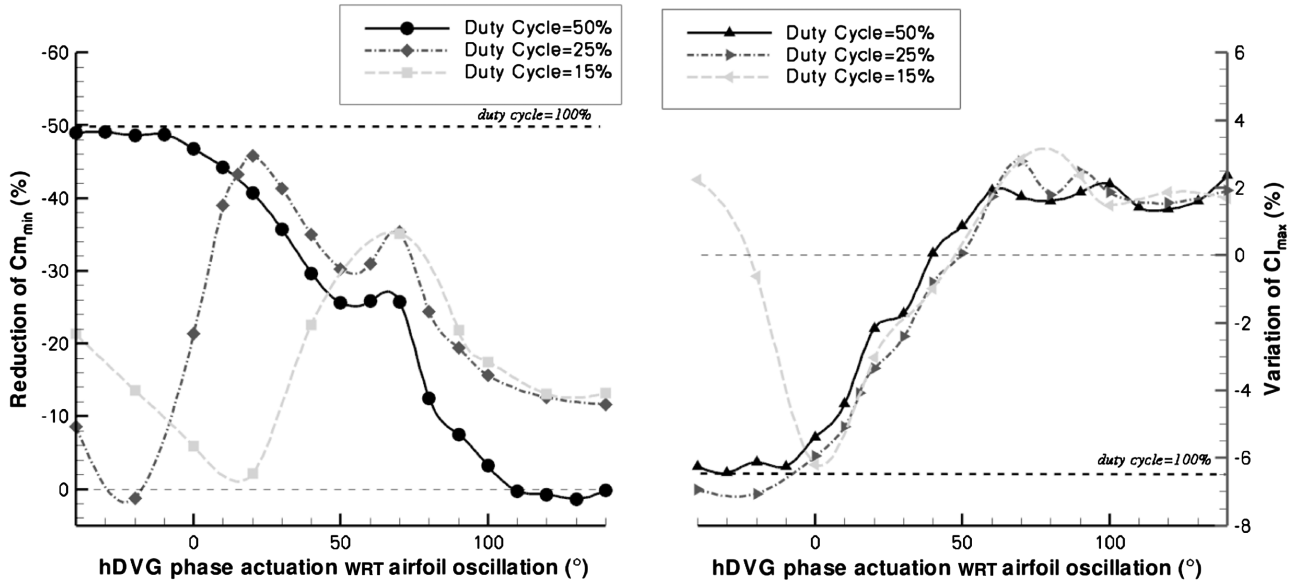

Fig. 16 Synthesis of DVG effectiveness for $hDVG = 1.5$ mm and several duty cycles with respect to (WRT) DVG actuation phase: (left) pitching moment; (right) lift.

Another way of evaluating the dynamic stall properties and the dynamic stall alleviation of a device is to plot the nondimensionalized aerodynamic damping (S/S*) also known as the Liiva criterion, of which a detailed description can be found in [25]. A more recent application and description is also available in [26]. Indeed, the net work done by the airfoil on the surrounding air is proportional to the integral of the pitching-moment coefficient over angle of attack variation (i.e., the area enclosed by the $Cm(\alpha)$ curve). For a counterclockwise loop of Cm, the net work is positive. In the case of a clockwise loop, the contribution of the corresponding area is negative, meaning that energy is extracted by the airfoil model from the flow. When this criterion is negative, the negative area is dominant, meaning that the airfoil body extracts energy from the flow and the configuration is unstable. When the criterion is positive, the airfoil provides energy to the flow and the configuration is stable. When the flow remains attached during all the oscillation cycle, the value of the criterion is close to 1.

The nondimensional aerodynamic damping (S/S^*) is plotted in Fig. 17 for the different duty cycles and for varying phase actuations. The reference value of this criterion is represented by the bottom dashed line for the reference case ($hDVG = 0$ mm). The reference case experiences a deep dynamic stall, and consequently, the value of the Liiva criterion is strongly negative ($S/S^* = \sim -1.5$). The case for static deployment of the DVGs at a height $hDVG = 1.5$ mm (duty cycle = 100%) is represented by the top dashed line. In this case, the dynamic stall is strongly reduced and the negative loop of the pitching moment has mostly vanished, consequently a positive aerodynamic damping is achieved ($S/S^* = \sim 0.5$). When the DVGs are activated, for almost all actuation phases and the three duty cycles investigated, the value of the Liiva criterion is higher than for the reference case, indicating that dynamic stall has been reduced. The value of the Liiva criterion and its evolution with phase is in good agreement with the previous observation on the pitching-moment and lift coefficient. For large reductions of the negative pitching-moment peak, the value of the Liiva criterion is high, and low values are obtained for limited or no gain in negative pitching-moment peak. A region of positive Liiva criterion (stable) is even achieved with a duty cycle equal to 50% and an early deployment of the DVGs (phase < 50 deg). For such a deployment scheme, a positive aerodynamic damping similar to the duty cycle = 100% case is reached, showing the advantage of a dynamic deployment in this case. The local optimum for the three duty cycles around a phase actuation equal to 70 deg can also clearly be seen. For this phase value, a Liiva criterion around zero is reached.

For the three duty cycles considered, a local optimum thus exists at a phase actuation equal to 70 deg (Fig. 16). This actuation phase corresponds to DVGs deployment just before the maximum angle of attack and the dynamic stall appearance. When the DVGs are deployed at this time in the cycle, it appears that the duration of the deployment is of secondary importance and similar pitching-moment and lift characteristics are obtained for the different duty cycles. To investigate the DVGs action on the flow, pressure distributions for different instants during the DVGs deployment are presented in Fig. 18 for a duty cycle equal to 25% and compared to the pressure distributions of the reference case. The left plot presents the pressure distributions during the upstroke just before the DVGs deployment. At this time, the controlled case and the reference case are obviously very similar; the flow is attached, and a large suction peak is present at the leading-edge. The center plot presents the same comparison a short time after the deployment, just after the maximum angle of attack. At this instant, the flow separates from the leading edge for the reference case, and a large dynamic stall vortex is emitted and shed to the trailing edge. For the controlled case, the flow remains attached in the leading-edge region where a strong suction peak is preserved. The airfoil experiences a trailing-edge stall as shown by the pressure plateau from $x/c = 0.35$, but the DVGs prevent the flow from separating upstream of the quarter-chord of the airfoil. The attached flow at the leading edge produces a much higher lift than in the reference case and also leads to a much smaller negative pitching moment.

Indeed, most of the airfoil aerodynamic loading is in the leading-edge region, promoting a nose-up pitching motion. The right plot, finally, presents the pressure distributions comparison just after the DVGs retraction, which happens in this case during the downstroke. The flow is fully separated for the reference case, when it remains partially attached at the leading edge in the controlled case. In fact, the flow remains attached at the leading edge during all of the downstroke, even after the DVGs have been retracted, benefiting from the attached flow history. Obviously, a much higher amount of lift is generated, and the pitching moment is increased. To conclude, the DVGs have a local action at the leading edge, preventing the flow from separating in this region. In addition, when the DVGs are deployed at the proper instant, the leading-edge attached flow during the deployment benefits from the aerodynamic characteristic of the airfoil all over the airfoil oscillation cycle, thanks to the history effect.

D. Negative Pitching Moment/Maximum Lift Compromise

As presented in the previous sections, the dynamic stall control using DVGs allows several compromises between maximum lift and minimum negative pitching moment to be found depending on the control scheme. In addition to square inputs for DVGs deployment previously presented, several other deployment schemes were tested, such as half-sine inputs. Comparison of minimum negative pitching moment versus maximum lift for square and half-sine input signals is presented in Fig. 19 for a duty cycle equal to 50% and varying actuation phases.

It can be clearly seen that maximum lift varies linearly with respect to the minimum pitching moment in the central part of the plot. In this region, a very good agreement between square and sine signals input is observed. It first shows that deploying the DVGs progressively with a sine motion brings no more benefit than a simpler instantaneous deployment. This region is also bounded by the maximum pitching moment reachable and the maximum lift coefficient reachable. Such a plot, therefore, provides valuable and

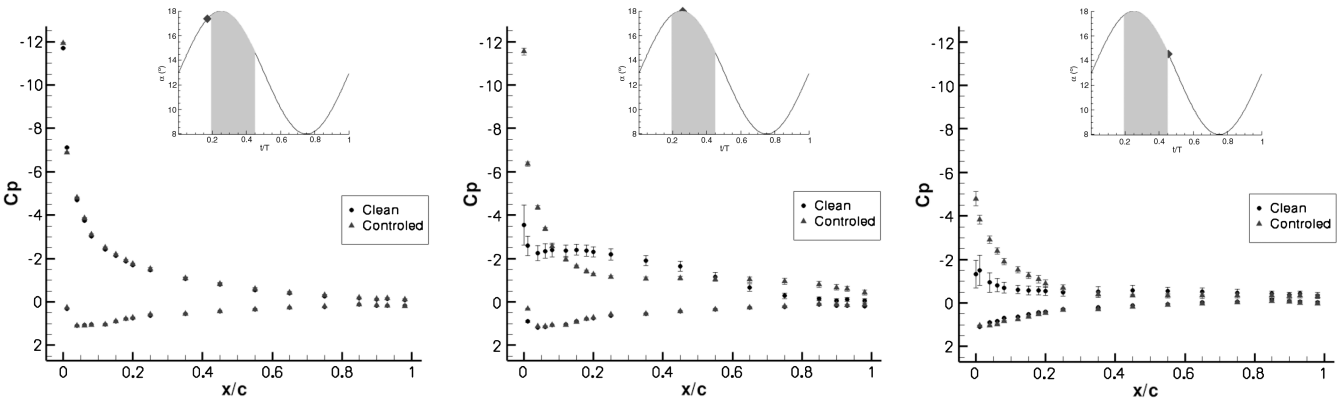

Fig. 18 Pressure distributions comparison for different instants in the cycle between the reference case and controlled case ($hDVG = 1.5$ mm, phase = 70 deg, duty cycle = 25%).

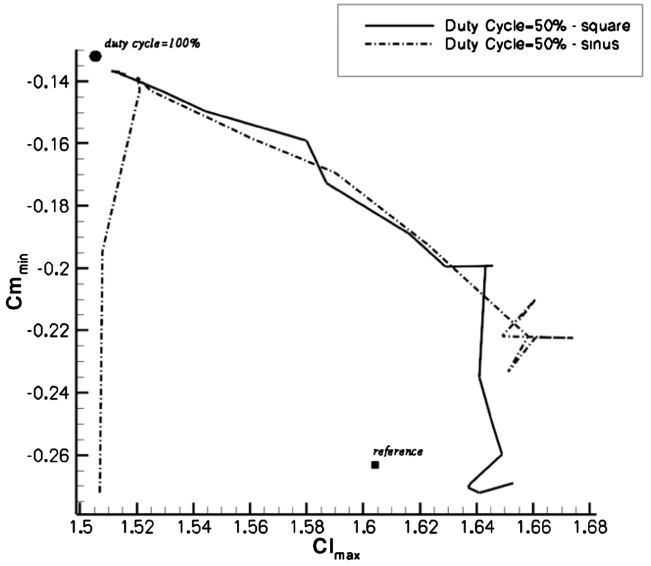

Fig. 19 Negative pitching moment/maximum lift comparisons for two different deployment schemes.

useful information for the DVG deployment scheme to be applied depending on the objective on the maximum lift sustain and the negative pitching-moment peak reduction.

VII. Conclusions

An innovative active flow control device for dynamic stall penalties alleviation has been designed and tested at ONERA. The device is a row of deployable vortex generators implemented at the leading edge of the OA209 airfoil. Significant static stall and dynamic stall reductions have been experimentally demonstrated in the ONERA low-speed F2 wind tunnel.

For static stall, a delay of up to 3 deg of the static stall angle of attack was achieved. Results show that static stall delay is obtained for a small deployable vortex generator (DVG) height equal to 0.3 mm, but that much higher delays are obtained for $hDVG = \sim 1.5$ mm. This delay is obtained by alleviating the leading-edge stall while promoting the trailing-edge separation. Therefore, the static stall delay is achieved at the price of a reduction of maximum lift.

For dynamic stall, a large reduction of the negative pitching moment is shown. Up to 55% of $Cm_{\min}$ reduction is achieved when DVGs are deployed all over the airfoil oscillation cycle for an optimal DVG height equal to 1.5 mm. A loss of maximum lift of 10% is also observed. The analysis of various DVG deployment schemes shows that various compromises between minimum negative pitching-moment peak and maximum lift can be reached. When DVGs are deployed sufficiently soon before the occurrence of dynamic stall, a very large reduction of the negative pitching moment is reached, but a loss of maximum lift is also obtained. A good compromise exists for an actuation phase equal to 70 deg, for which a reduction of 30% of the negative pitching moment is achieved, with a limited loss of 2% of maximum lift. Duty-cycle optimization was performed, and it was demonstrated that these results can be obtained for a duty cycle down to 15%, ensuring limited drag penalties due to DVGs. Finally, it was shown that DVGs act mostly in the leading-edge region where the dynamic stall is prevented from occurring by ensuring an attached flow at the leading edge all over the airfoil oscillation cycle.

If the effectiveness of DVGs is demonstrated for two-dimensional dynamic stall, some questions remain open and must be investigated. The present work has been done for a reduced frequency of 0.1 for a particular dynamic stall event, and the effectiveness of the DVG system to control all types of dynamic stall for lower and higher reduced frequencies remains to be demonstrated. The vortex convection time is, however, an order of magnitude quicker than the pitching-motion frequency, and a similar effectiveness of the DVGs is, thus, expected for other frequencies. The physics of the DVG influence on the flow needs also to be understood. The paper is focused on the most effective case, with DVGs deployed at a height of the order of that of the separating shear layer, but more limited dynamic stall alleviation has also been identified at DVG heights of the same order as the boundary-layer thickness; this remains to be more deeply investigated. For that, numerical studies are underway and expected to provide valuable information about the DVGs' vortex generation process. In particular, the influence of the DVG thickness is shown in these numerical studies as a key factor for the DVG effectiveness. Additional time-resolved particle image velocimetry measurements performed by the DLR, German Aerospace Research Center during the wind-tunnel tests of the present study are expected to bring a close insight into the flowfield and the dynamic stall vortex formation and alleviation. DVGs should also be tested in future wind-tunnel tests for other dynamic stall and aerodynamic conditions to verify the robustness of the system.

Acknowledgments

The authors would like to thank all the ONERA teams that have been involved in the model design, manufacturing, wind-tunnel test preparation and execution, and experimental results postprocessing. The DLR, German Aerospace Research Center is also thanked for participation in the wind-tunnel tests in the framework of the ONERA–DLR SIMCOS project.

References

[1] Karim, M., and Acharya, M., "Suppression of Dynamic Stall Vortices over Pitching Airfoils by Leading-Edge Suction," *AIAA Journal*, Vol. 32, No. 8, Aug. 1994, pp. 1647–1655. doi:10.2514/3.12155

[2] Greenblatt, D., and Wygnanski, I., "The Control of Flow Separation by Periodic Excitation," *Progress in Aerospace Sciences*, Vol. 36, No. 7, 2000, pp. 487–545. doi:10.1016/S0376-0421(00)00008-7

[3] Greenblatt, D., and Wygnanski, I., "Effect of Leading-Edge Curvature and Slot Geometry on Dynamic Stall Control," *AIAA 1st Flow Control Conference*, AIAA, June 2002.

[4] Post, M., and Corke, T., "Separation Control Using Plasma Actuators: Dynamic Stall Vortex Control on Oscillating Airfoil," *AIAA Journal*, Vol. 44, No. 12, Dec. 2006, pp. 3125–3135. doi:10.2514/1.22716

[5] Chandrasekhara, M., Wilder, M., and Carr, L., "Compressible Dynamic Stall Control Using Dynamic Shape Adaptation," *AIAA Journal*, Vol. 39, No. 10, Oct. 2001, pp. 2021–2024. doi:10.2514/2.1196

[6] Geissler, W., Dietz, G., Mai, H., Junker, B., and Lorkowski, T., "Dynamic Stall Control Investigations on a Full Size Chord Blade Section," 30th European Rotorcraft Forum, Marseille, France, Paper No. 16, 14–16 Sept. 2004.

[7] Chandrasekhara, M., Martin, P., and Tung, C., "Compressible Dynamic Stall Control Using a Variable Droop Leading-Edge Airfoil," *Journal of Aircraft*, Vol. 41, No. 4, July–Aug. 2004, pp. 862–869. doi:10.2514/1.472

[8] Carr, L. W., and McAlister, K. W., "The Effect of a Leading Edge Slat on the Dynamic Stall of an Oscillating Airfoil," AIAA Paper 1985-2533, Oct. 1983.

[9] Martin, P., Wilson, J., Berry, J., Wong, T. C., Moulton, M., and McVeigh, M., "Passive Control of Compressible Dynamic Stall," *26th AIAA Applied Aerodynamics Conference*, AIAA Paper 2008-7506, Aug. 2008.

[10] Mai, H., Dietz, G., Geissler, W., Richter, K., Bosbach, J., Richard, H., and de Groot, K., "Dynamic Stall Control by Leading-Edge Vortex Generators," *Journal of the American Helicopter Society*, Vol. 53, No. 1, Jan. 2008, pp. 26–36. doi:10.4050/JAHS.53.26

[11] Magill, J., and McManus, K., "Control of Dynamic Stall Using Pulsed Vortex Generators Jets," AIAA Paper 1998-0675, 1998.

[12] Singh, C., Peake, D. J., Kokkalis, A., Khodagolian, V., Coton, F., and Galbraith, R., "Control of Rotorcraft Retreating Blade Stall Using Air-Jet Vortex Generators," *Journal of Aircraft*, Vol. 43, No. 4, 2006, pp. 1169–1176. doi:10.2514/1.18333

[13] Osborn, R., Kota, S., Hetrick, J., Geister, D., Tilmann, C., and Joo, J., "Active Flow Control Using High-Frequency Compliant Structures,"

Journal of Aircraft, Vol. 41, No. 3, May–June 2004, pp. 603–609. doi:10.2514/1.111

[14] Barth, T., Scholz, P., and Wierach, P., "Flow Control by Dynamic Vane Vortex Generators Based on Piezoceramic Actuators," *AIAA Journal*, Vol. 49, No. 5, May 2011, pp. 921–931. doi:10.2514/1.J050378

[15] Seshagiri, A., Cooper, E., and Traud, L., "Effects of Vortex Generators on an Airfoil at Low Reynolds Numbers," *Journal of Aircraft*, Vol. 46, No. 1, Jan.–Feb. 2009, pp. 116–122. doi:10.2514/1.36241

[16] Le Pape, A., Pailhas, G., David, F., and Deluc, J.-M., "Extensive Wind Tunnel Measurements of Dynamic Stall Phenomenon for the Oa209 Airfoil Including 3D Effects," *33rd European Rotorcraft Forum*, Paper 10, Kazan, Russia, Sept. 2007.

[17] Richez, F., Gleize, V., Mary, I., and Basdevant, C., "Near Stall Simulation of the Flow Around an Airfoil Using Zonal RANS/LES Coupling Method," *Computers and Fluids*, Vol. 37, No. 7, 2008, pp. 857–866. doi:10.1016/j.compfluid.2007.03.016

[18] Costes, M., Gleize, V., Le Pape, A., and Richez, F., "Numerical Investigation of Laminar/Turbulent Transition Effects on the Dynamic Stall of an Oscillating Airfoil," *American Helicopter Society Specialist Conference on Aeromechanics*, San Francisco, CA, Jan. 23–25, 2008.

[19] Richter, K., Le Pape, A., Knopp, T., Costes, M., Gleize, V., and Gardner, A., "Improved Two-Dimensional Dynamic Stall Prediction with Structured and Hybrid Numerical Methods," *Journal of the American Helicopter Society*, Vol. 56, No. 4, Oct. 2011, pp. 1–12. doi:10.4050/JAHS.56.042007

[20] Lin, J., "Review of Research on Low-Profile Vortex Generators to Control Boundary-Layer Separation," *Progress in Aerospace Sciences*, Vol. 38, Nos. 4–5, 2002, pp. 389–420. doi:10.1016/S0376-0421(02)00010-6

[21] Godard, G., and Stanislas, M., "Control of a Decelerating Boundary Layer. Part 1: Optimization of Passive Vortex Generators," *Aerospace Science and Technology*, Vol. 10, No. 3, 2006, pp. 181–191. doi:10.1016/j.ast.2005.11.007

[22] McCroskey, W. J., "Dynamic Stall of Airfoils and Helicopter Rotors," AGARD Rept. 595, Neuilly sur Seine, France, 1972.

[23] Joubert, G., Le Pape, A., and Huberson, S., "Numerical Study of Flow Separation Control over a OA209 Airfoil Using Deployable Vortex Generator," *49th AIAA Aerospace Sciences Meeting*, AIAA Paper 2011-1044, 2011.

[24] Joubert, G., Le Pape, A., Heine, B., and Huberson, S., "Investigation of Dynamic Stall Control by Deployable Vortex Generator Using Time-Resolved PIV Analysis and URANS Computations," *37th European Rotorcraft Forum*, Paper 146, Italy, 2011.

[25] Liiva, J., "Unsteady Aerodynamic and Stall Effects on Helicopter Rotor Blade Airfoil Sections," *Journal of Aircraft*, Vol. 6, No. 1, 1969, pp. 46–51. doi:10.2514/3.44000

[26] Klein, A., Richter, K., Altmikus, A., Lutz, T., and Krämer, E., "Unsteady Criteria for Rotor Blade Airfoil Design," *35th European Rotorcraft Forum*, Paper 1216, Hamburg, Germany, 2009.

A. Naguib
Associate Editor